Investigating Derivatives of Tanshinone IIA Sulfonate Sodium and Chloroxine for Their Inhibition Activities against the SARS-CoV-2 Papain-like Protease

Xin Chen,◆ Ke Chen,◆ Zhaoyong Zhang,◆ Peilan Wei,◆ Lu Zhang, Yunxia Xu, Qili Lun, Yanhong Ma, Fang Wu, Ying Zhang, Yanqun Wang, Jincun Zhao,* Yaoqi Zhou,* Jian Zhan,* and Wei Xu*

ACCESS | Metrics & More | Article Recommendations | Supporting Information
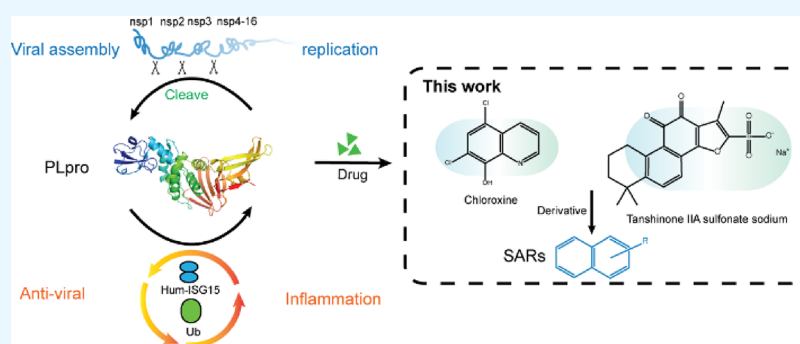
ABSTRACT: SARS-CoV-2 has caused a global pandemic of COVID-19, posing a huge threat to public health. The SARS-CoV-2 papain-like cysteine protease (PLpro) plays a significant role in virus replication and host immune regulation, which is a promising antiviral drug target. Several potential inhibitors have been identified in vitro. However, the detailed mechanism of action and structure−activity relationship require further studies. Here, we investigated the structure−activity relationships of the series of derivatives of tanshinone IIA sulfonate sodium (TSS) and chloroxine based on biochemical analysis and molecular dynamics simulation. We found that compound **7**, a derivative of chloroxine, can disrupt PLpro-ISG15 interaction and exhibits an antiviral effect for SARS-CoV-2 variants (wild type, delta, and omicron) at the low micromolar level. These studies confirmed that inhibiting PLpro-ISG15 interaction and, thus, restoring the host's innate immunity are effective methods for fighting against viral infection.

■ INTRODUCTION

The global epidemic of COVID-19 caused by the new coronavirus SARS-CoV-2 infection has led to the great harming to the economy and human health. This is the third worldwide pandemic caused by the coronavirus after SARS-CoV and MERS-CoV.[1] The clinical manifestations of patients infected with SARS-CoV-2 range from asymptomatic or mild infection to acute lung inflammation and pneumonia and are more common in the elderly and patients with comorbidities.[2−4] Although the symptoms are milder than those of SARS-CoV and MERS-CoV, SARS-CoV-2 spreads faster.[5] This new type of coronavirus is also more contagious and pathogenic[6] than influenza virus despite similar symptoms such as fever, cough, and pneumonia. Initially, some old antiviral drugs such as remdesivir (targeting RNA-dependent RNA polymerase, RdRP), chloroquine (targeting spike protein), and tocilizumab (targeting human IL-6 receptor) were tested directly on COVID-19 patients.[7−10] Although they have a noticeable antiviral effect, their efficacy remains controversial.[11]

One strategy for developing effective antiviral strategies is to target key factors in the viral life cycle, particularly, important viral enzymes such as RdRP, main protease (Mpro/3CLpro), and papain-like protease (PLpro).[12] Luteolin was reported to bind to multiple targets of SARS-CoV-2 PLpro, spike, and RNA-dependent RNA polymerase (RdRP) but with its actual efficacy unknown.[13−16] One recent successful drug molnupiravir was approved to target RdRP.[17−19] However, more drugs for additional targets are clearly needed to fight against this fast-evolving virus. Here we will focus on SARS-CoV-2 PLpro.

SARS-CoV-2 PLpro is the main protease encoded by nsp3 with an N-terminal ubiquitin-like (UBL) domain and a C-

Table 1. In Vitro Inhibitory Activity of Analogues of Tanshinone IIA Sulfonate Sodium (TSS) as Inhibitors of PLpro Enzymatic Activity
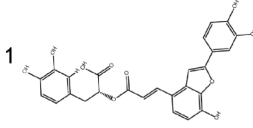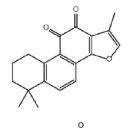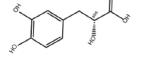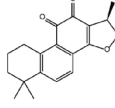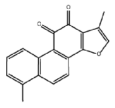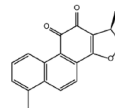
	Chemical structure	IC_{50} (μM)		Chemical structure	IC_{50} (μM)
1		>93.7	4		none
2		>100	5		>100
3		none	6		68.3
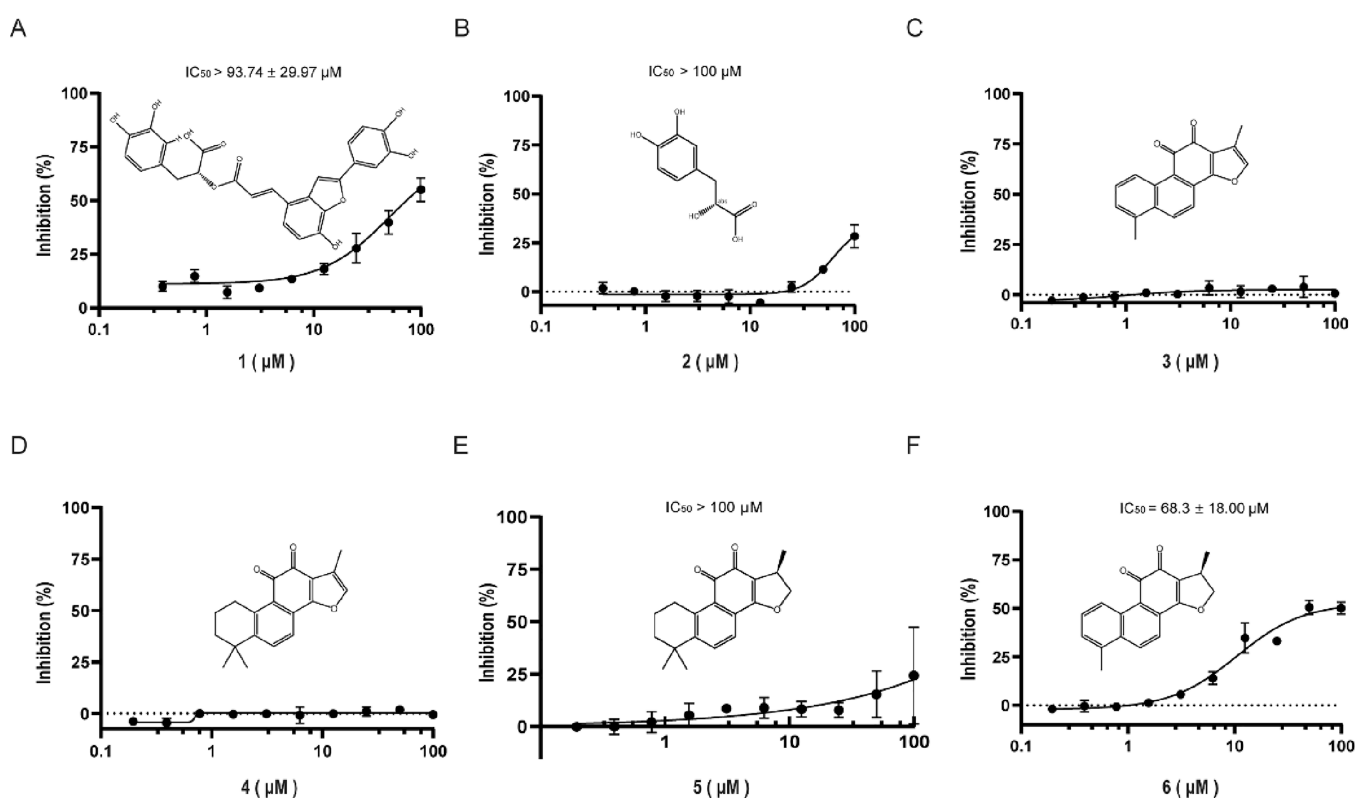
Figure 1. In vitro enzymatic activity of analogues of tanshinone IIA sulfonate sodium (compounds **1−6**) as a function of the compound concentration in μM. Activity analysis of compounds based on the inhibition assay of protease activity of AMC probes. The 50% inhibition concentrations for compounds **1** (A) and **6** (F) are lower than 100 μM. Others showed poor (B, E) or no inhibition (C, D).

terminal ubiquitin-specific protease (USP) domain. It can cleave the viral polyprotein to form nsp1, nsp2, and nsp3 and interact with ubiquitin or ISG15 from host proteins[20] for reducing the host's innate immunity.[21,22] This dual role of PLpro makes it an attractive drug target for developing effective antiviral drugs and regulating virus−host immunity interactions. Because SARS-CoV-2 PLpro is highly similar to the SARS-CoV PLpro with 83% of amino acid similarity and an identical active site,[23] many SARS-CoV PLpro inhibitors can inhibit SARS-CoV-2 PLpro as well.[20,24] One example is GRL0617, which can interact with either Tyr268 of SARS-CoV-2 PLpro or Tyr269 of SARS-CoV PLpro.[24] GRL0617 can inhibit SARS-CoV-2 PLpro with ~2 μM IC_{50} values but poorer

antiviral activity (Vero E6 and Caco2-hACE2: EC_{50} values around 20 μM).[25−27] GRL0617 analogues such as Jun9-72-2 and Jun9-75-4 were found with higher enzymatic inhibition and antiviral activity.[27] Furthermore, GRL0617 and its analogues form hydrophobic interactions between their naphthalene ring and Tyr268 of SARS-CoV-2 PLpro.[27] Therefore, GRL0617 mainly binds around the active pocket of PLpro.

Recently, we discovered two new PLpro inhibitors: tanshinone IIA sulfonate sodium (TSS) and chloroxine, with IC_{50} lower than 10 μM after screening a library of clinically approved drugs.[28] The structure of these two compounds is quite different from GRL0617 and its analogues. The naphthyl
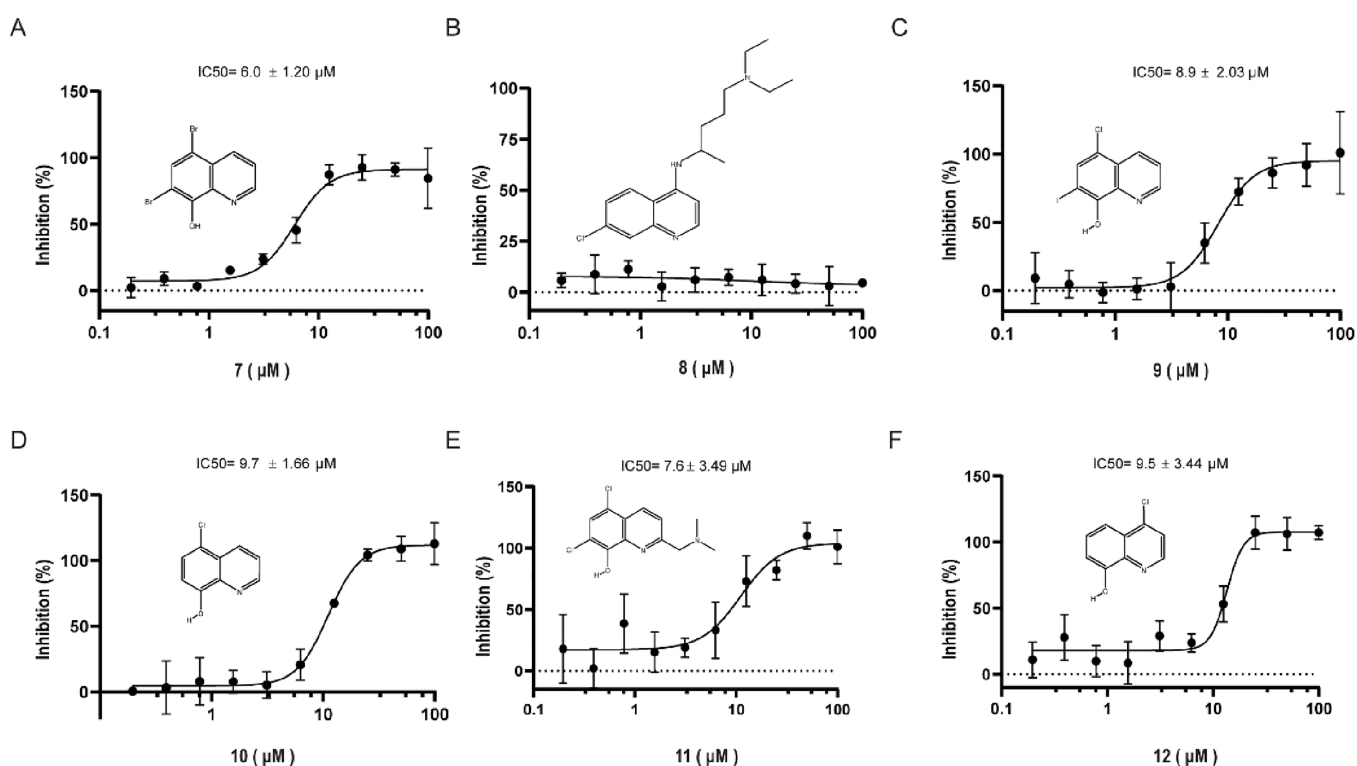
Figure 2. In vitro PLpro-ISG15 binding inhibition of chloroxine analogues (compounds **7−12**) as a function of the compound concentration in μM. All compounds in this group have similar inhibitory activities as chloroxine except compound **8** (B) with no inhibitory activity. In addition, compound **7** (A) showed good inhibitory activity followed by compound **11** (E). The inhibitory activities of compounds **9** (C), **10** (D), and **12** (F) were highly similar.

Table 2. In Vitro Inhibitory Activity of Analogues of Chloroxine as the Inhibitor of PLpro-ISG15 Binding Activity

	Chemical structure	IC$_{50}$ (μM)		Chemical structure	IC$_{50}$ (μM)
7		6.0	10		9.7
8		none	11		7.6
9		8.9	12		9.5

RESULTS AND DISCUSSION
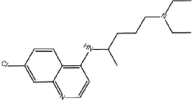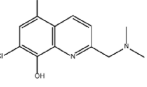
In Vitro Analysis of TSS Analogs by the Protease Activity Assay. We employed previously developed enzymatic activity[28] to examine inhibition of TSS analogues as TSS was found to inhibit enzymatic activity. Compounds **1−6**, like TSS, are derived from the natural product Danshen. The main component of Danshen is a cytochrome P450 (CYP) group of GRL0617, Jun9-72-2, and Jun9-75-4 is the key binding region to PLpro. Interestingly, TSS and chloroxine were substituted on the naphthalene ring. Based on this insight, we examined additional analogues of TSS and chloroxine to establish structure−activity relationships (SARs). Several analogues of chloroxine with lower than 10 μM IC$_{50}$ values were found.

inhibitor,[29] and most drugs are metabolized by CYP on liver microsomes in vivo. Thus, the drug metabolism rate for this cluster of drugs in vivo may be low. Although compounds **1** and **2** are different from the basic structure of TSS, they are derived from the main components of Danshen, and they were considered here as the same type of natural products. Table 1 and Figure 1 show the resulting IC$_{50}$ values for the derivatives of TSS (**1−6**). Most TSS derivatives are poor inhibitors or lack inhibition of enzymatic activities. The best TSS derivative (compound **6**) has an IC$_{50}$ value of 68 μM, compared to 1.65 μM TSS.

The above results highlighted the critical role of the sulfonyl group in inhibiting PLpro enzymatic activity. This is illustrated by the fact that compound **4** only differs from TSS by lacking the sulfonyl group. Without this sulfonyl group, compound **4**

completely lost the inhibition. Interestingly, removing the double bond in the epoxy group of compound **4** (compound **5**) leads to a partial restoration of inhibition, whereas introducing an additional aromatic ring to compound **5** (compound **6**) further improves inhibition. Also, removing the double bond in the epoxy group of compound **3** (compound **6**) leads to a significant recovery of inhibition. The partial inhibitory effects of compounds **1** and **2** indicated that phenolic acid compounds were another active ingredient in Danshen besides tanshinone. Among them, benzenediol may play an inhibitory role as an active group. It is further observed that its active components and active groups from the perspective of natural products are promising strategies for antiviral drug discovery. The above results suggest that tanshinone is the active compound skeleton in the natural product Danshen with a potential effect of inhibiting PLpro. Moreover, the sulfonic acid group has a significant effect on the skeleton, and the active conformation it participates in mainly affects the epoxy group directly connected to it in the skeleton.

In Vitro Analysis of Chloroxine Analogs by the Fluorescence Polarization Assay (FPA). We further employed the previously developed ISG15-binding assay[28] to examine inhibition of binding by chloroxine analogues as chloroxine was found to inhibit the binding between ISG15 and PLpro. The concentration dependence of binding inhibition for these compounds can be found in Figure 2A–F. Table 2 shows the IC_{50} value results of six chloroxine derivatives for their deISGylating activity of SARS-CoV-2 PLpro. The chemical structure of this cluster of compounds is relatively simple, so we mainly focus on its quinoline backbone and the substitution of different halogen atoms and the size of the side chain.

Most of these chloroxine analogues maintain chloroxine's inhibition ability with <10 μM IC_{50} values, except compound **8**. The corresponding concentration dependence of inhibition for these compounds can be found in Figure 2A–F. The active analogues all have a minor substitution/deletion relative to chloroxine. Substitution of two Cl atoms by Br leads to compound **7**, by one I to compound **9**, whereas removal of Cl leads to compound **10** and shift of a Cl position to compound **12**. Compound **11**, on the other hand, introduced a triethylamine group. With quinoline as the main skeleton, various groups can be added or switched to maintain the inhibitive activity, suggesting that quinoline is directly involved in binding inhibition. The inactivity of compound **8** further suggests that the binding of quinoline may be affected by the steric hindrance effect of the giant side chain.

Docking and Molecular Dynamics. To further understand the molecular mechanisms of these analogues, we performed docking and molecular dynamics simulations as we have done previously.[28] Compounds **1**–**12** were docked onto PLpro by AutoDock Vina,[30] and their interaction sites were analyzed. The docked complex structures were subjected to molecular dynamics simulation for relaxing docked structures.

Table S1 shows the best docking scores along with the locations of the ligands. We found that compounds **1**–**6** were mainly located in the catalytic pocket of PLpro, while **7**–**12** (except **8**) mainly interacted with the binding interface of PLpro and ISG15 (Figure S1 and Figure 5B). This is mostly consistent with the fact that compounds **1**–**6** and **7**–**12** are the analogues of TSS (pocket binder) and chloroxine (interface binder), respectively. Docked conformations were minimized

and subjected to 200 ns MD simulations for examining their binding stability and interaction details.

Figure S3A–F shows the time dependence of conformation stability of TSS analogues by the MD simulations. Figure S2 shows a detailed view of the interaction of all compounds with PLpro. Among compounds **1**–**6**, only compound **6** (Figure S3F) had weak stable binding to the catalytic pocket of PLpro, which was consistent with our enzymatic activity analysis (Figure 1). In particular, similar to TSS, compound **6** mainly utilizes its aromatic ring through π–π stacking near the Tyr268 residue. Unlike TSS, the cation–π interaction with the Arg166 residue is weaker (Figures S3F and S4F). Compounds **1**–**6** could not achieve stable binding with PLpro due to the lack of hydrophilic sulfonic acid groups, considering the fact that compound **4** only differs from TSS by a sulfonic group. Although compound **6** is mainly binding at the catalytic pocket, the binding conformation of compound **6** is flexible with large fluctuation in distances (Figures S3F and S4F).

Figure S3G–L shows the results of MD simulations for chloroxine analogues (compounds **7**–**12**). Similar to chloroxine,[28] there appear to have two-state binding conformations at the ISG15-PLpro interface for those compounds with inhibition activities (**7**, **9**, **10**, **11**, and **12**) based on distance fluctuation. For compound **8**, although it has an initial docking binding mode in the activity pocket (Figure S1G), the conformation is not stable in the MD simulation (data not shown). This instability may be due to the bulky side chain introduced in compound **8** (Figure 2B). The interface binders are mainly anchored by the Arg65 residue near the interface through cation–π interactions as chloroxine (Figure S3H–L). For example, after the Cl atom substitution of chloroxine is replaced by Br atom substitution (Figure 3), compound **7**
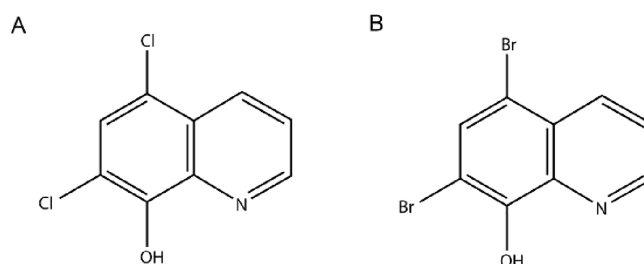
Figure 3. Comparing the chemical structures of chloroxine (A) and compound **7** (B); the two share a quinolone ring but have different halogen atom substitutions at C-5 and C-7.

adopts the same binding conformation as the state 1 of chloroxine[28] but is more stable (Figure 5B and Figure S3H). The bound conformation undergoes a transition from two states (states 1 and 2) to a single state (state 1). In this conformation, the halogen atoms are deeply buried in the protein pocket and possibly because the Br atoms are larger than the chlorine atoms, resulting in a stronger interaction with the protein (Figures S3H and S4H). Compared to compound **7**, compound **9** is actually buried deeper, possibly because the I atom is too large and the ring plane cannot reach fully to the orientation of state 1 (Figures S3I and S4I).

Non-binding ligands (compounds **7**–**12**) on the catalytic binding pocket could be viewed as docking decoys, in respective to those binding ligands (compounds **1**–**6**) on the binding pocket. MD simulations of these decoy ligands were dissociated from the pocket. An example of compound **7**
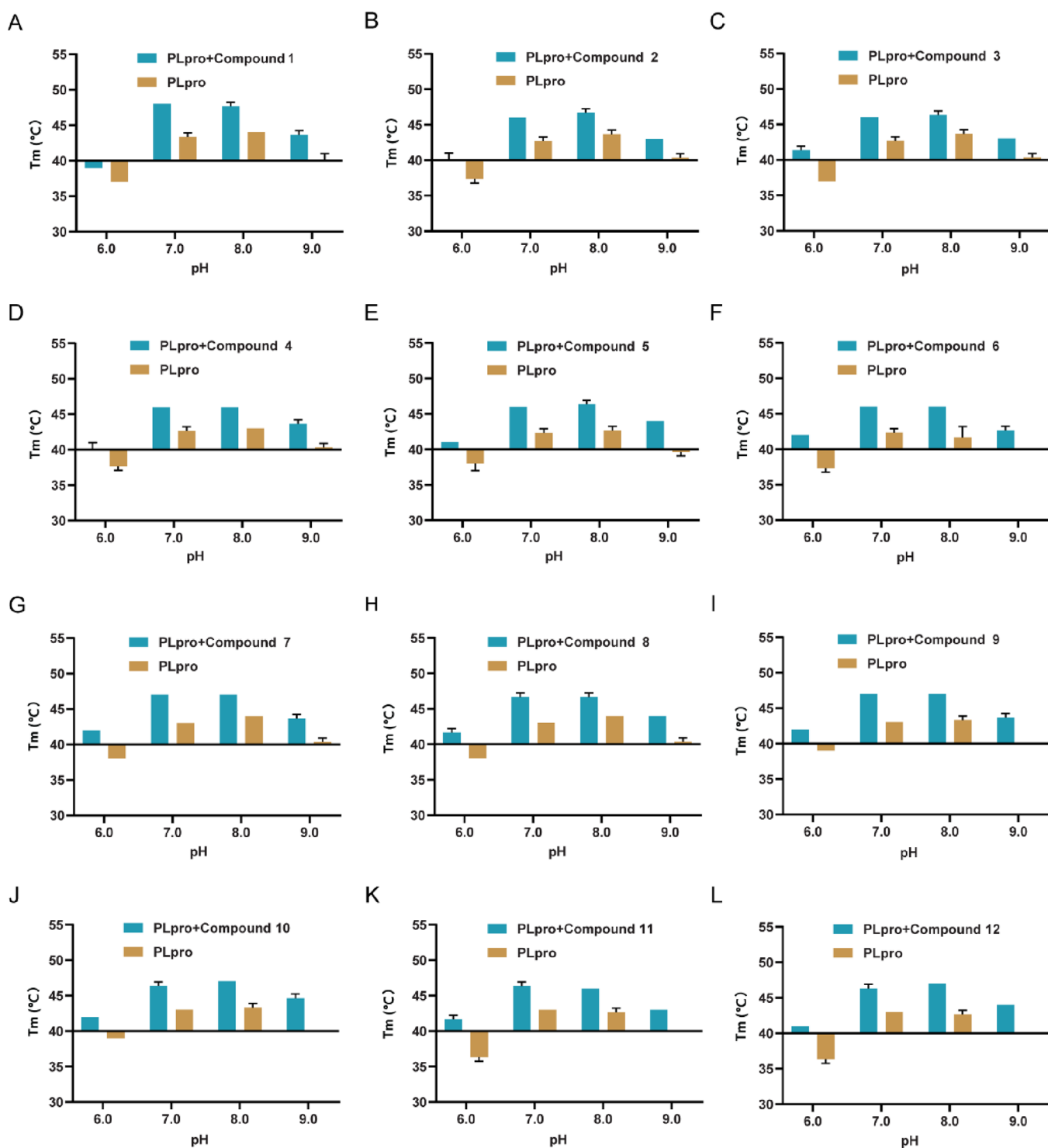
Figure 4. Stability change of PLpro in the presence of ligands at different pH values (A–L) for compounds **1–12**. The determination of the thermal stability of the protein was done on a real-time PCR system by the thermal shift assay (TSA) method.

dissociating from the initial structure near the pocket is illustrated in Figures S3G and S4G. By comparison, the docking results for compounds **1–6** are dominated by the in-pocket conformations.

To further confirm our findings, we repeated two more MD runs for each MD setup with stable observed binding events. Figure S7 shows three independent MD simulations for the three most interesting compounds **7**, **9**, and **11**. The results for multiple runs for these three compounds confirmed stable

binding at the interface. We noted that compound **7** in run 3 adopted a deeply buried state 1-type binding mode with a rotation of the ligand around the normal vector of the molecular plane.

Interactions between PLpro and Its Inhibitors. Stability changes upon ligand addition provide a measure of interactions between PLpro and its inhibitors. Typically, we should observe an increase in melting temperature (Tm) upon binding, except that combining with other destabilizing effects
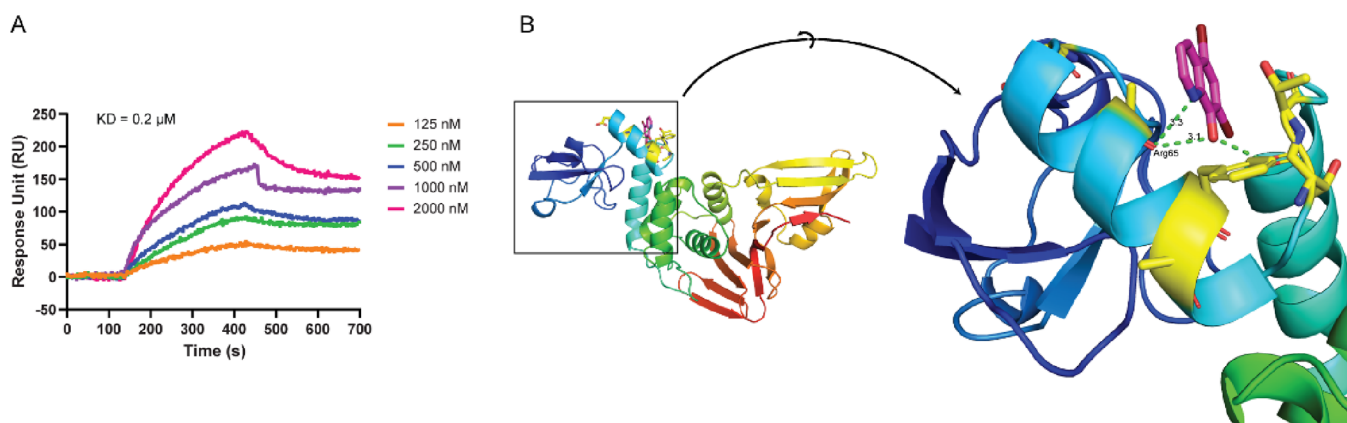
Figure 5. Binding of compound **7** to the PLpro. (A) Binding affinity was measured by surface plasmon resonance, and the equilibrium response unit was plotted against the compound concentration. The estimated K_D is 0.2 μM. (B) The docking results of compound **7** with PLpro showed that it was located at the PLpro-ISG15 interaction interface. Compound **7** has a hydrogen bond interaction with the Arg65 residue, and its distance is around 3 Å.

such as pH may produce a different outcome. The thermal melting curves when PLpro is mixed with compounds **1−12** are shown in Figure S5 along with the changes of Tm values at pH 6.0, 7.0, 8.0, and 9.0, as shown in Figure 4. PLpro has an optimal stability at pH values between 7.0 and 8.0, and there is an increase in Tm values in the presence of ligands in most cases (Figure S5B,C). It should be noted that all ligands improve PLpro stabilities, regardless of specific or non-specific inhibition. This indicates that stability change is not a useful tool to indicate specific inhibition.

Because compound **7** has the best IC_{50} value for disrupting ISG15-PLpro interactions (Table 2), we measured its binding affinity to PLpro for further validation. Results from surface plasmon resonance (SPR) indicate an estimated affinity of 0.2 μM (Figure 5A). In addition, it was found by docking that compound **7** was firmly anchored at the PLpro-ISG15 interaction interface by the Arg65 residue through the hydrogen bond (Figure 5B).

Antiviral Assays. To further validate the antiviral activity with authentic virus, compound **7** was performed on cell-based assays infected with authentic SARS-CoV-2 wild type, delta, or omicron variants. We observed a decrease in authentic virus infections in cells in a dose−response manner (Figure 6). A significant decrease in intracellular virus could be observed at a concentration of 11.1 μM or above. Meanwhile, the inhibitory effect of imatinib[31] in the positive control was observed when the drug concentration was greater than 15 μM (Figure S6). Compound **7** has an inhibitory effect on WT, delta, and omicron of SARS-CoV-2 and all inhibited virus infections at low micromolar concentrations. The EC_{50} values of compound **7** for WT, delta, and omicron inhibition were 4.59, 2.70, and 2.98 μM, respectively. The cytotoxicity of compound **7** in Vero E6 cells was determined by the CCK-8 method, and the results showed that its 50% cytotoxicity concentration was greater than 800 μM (Figure 6B). This suggests that the actual antiviral level of compound **7** is consistent with our observed biochemical activity and binding properties.

■ CONCLUDING REMARKS

PLpro, one of the proteases of SARS-CoV-2, plays a key role in viral self-assembly and host antiviral immune response, and it is a promising antiviral drug target. As the newly reported PLpro inhibitors, TSS and chloroxine are significantly different from

previously reported inhibitors in the chemical structure. Thus, it would be interesting to investigate TSS and chloroxine analogues. We showed that substitutions or removal of chlorine in chloroxine analogues makes minor changes to inhibition capability, whereas removal of the sulfonate group is detrimental to inhibition of enzymatic activity.

We found that aromatic naphthyl and quinolone rings as active groups play a major role in the active conformation of SARS-CoV-2 PLpro. GRL0617 has been reported as a potential lead compound of PLpro inhibitors for ISG15-PLpro binding.[26,32,33] Here, we also observed that the inhibitors in chloroxine derivatives share a naphthyl group with the compound GRL0617. The quinolone ring is re-recognized as the active backbone of PLpro inhibitors, and active compounds sharing the quinolone ring mainly target the PLpro-ISG15 interaction interface through the Arg65 residue. The substitutions of halogen atoms on the C-3, C-5, and C-7 positions of the quinolone ring are involved in the active conformation of the binding interface. The number of substitutions of halogen atoms also seems to have some effects on its activity (Table 2). However, the substitution of the bulky branch at the C-3 position might force compound **8** to PLpro to be away from the binding interface due to the steric hindrance effect. Indeed, compound **8** is inactive in FPA analysis (Figure 2B).

For inhibition of PLpro cleavage, the conserved Tyr268 residue of PLpro and the Arg166 residue are the key residues for anchoring inhibitors. Moreover, the sulfonyl group occupies a critical position in the active conformation of the inhibitor, which may be related to its participation in the formation of the core ring and its effect on the side-chain formation, as suggested by the inactive compound **4** (TSS without the sulfonyl group) and sulfonation at the C-16 position of TSS (Table 1).

Overall speaking, we obtained a lead compound (compound **7**), which has a μM level of in vitro biochemical and cell-level antiviral activities. This compound shares the same skeleton as chloroxine but with a suitable bromine atom substituted at C-5 and C-7 positions.

Small molecule inhibitors have always been a main source of drugs due to their advantages of good oral availability and relatively low production cost compared to antibodies. Using derivatives of a lead compound and analyzing structure—
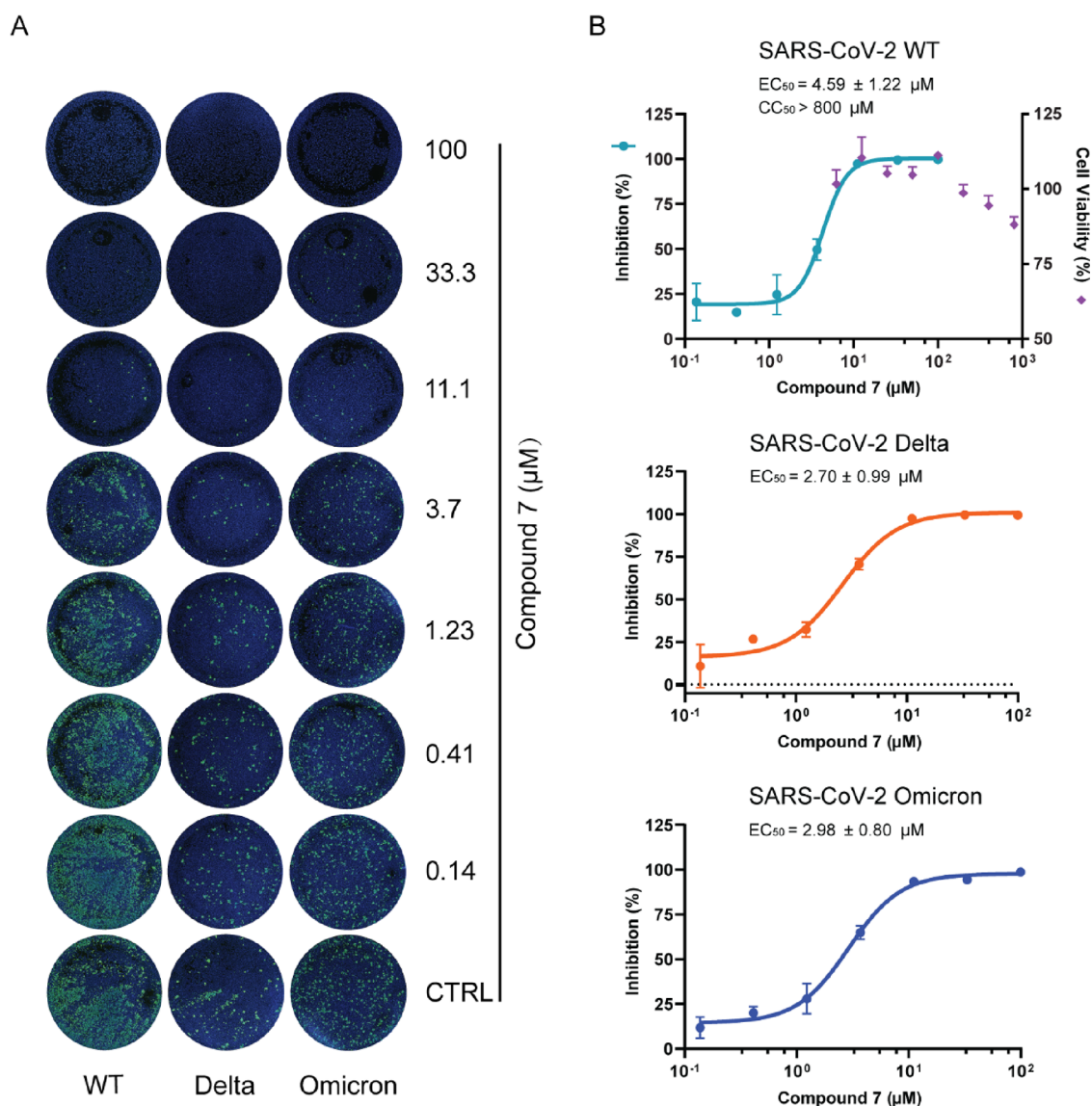
Figure 6. Antiviral assay based on the immunofluorescence assay (IFA). (A) Immunofluorescence microscopy was used to observe the inhibitory effect of compound 7 on SARS-CoV-2 infection. After 24 h of infection, cells were fixed, and intracellular SARS-CoV-2 specific NP levels were detected. Nuclei were stained with DAPI in blue. SARS-CoV-2 infected cells were stained in green. The scale bar is 500 μm. No compound was added to the control group under the same treatment. Imatinib was set as the positive control, and the drug concentration above 15 μM started to show an inhibitory effect. Results are representative of three biological replicates. (B) Inhibition of viral infection of Vero E6 cells by compound 7 was detected by the IFA, and the IFA results showed that compound 7 had an inhibitory effect on authentic SARS-CoV-2 wild type, delta, or omicron variants at the cellular level. The cytotoxicity (CC_{50}) of compound 7 on Vero E6 cells was analyzed by CCK-8 assays.

activity relations (SARs) of these derivations have proven effective tools in optimizing initial leads. Here, we examined several small molecule inhibitors of PLpro and the SAR analysis on these novel inhibitors, which are useful to further accelerate the development of more effective inhibitors to treat COVID-19.

■ EXPERIMENTAL SECTION

Virus and Cell. The SARS-CoV-2 strain (WT) used in this research was isolated from COVID-19 patients in Guangdong China passaged and titered on Vero E6 cells. The SARS-CoV-2 delta (B.1.617.2) strain was presented by Guangdong Provincial Center for Disease Control and Prevention, China. All work with SARS-CoV-2 was conducted in the Guangzhou Customs District Technology Center Biosafety Level-3 Laboratory.

Protein Expression and Purification. The SARS-CoV-2 PLpro gene was cloned into the expression vector pET28a with a C-terminal 6× His-tag. The recombinant plasmid was transformed into BL21 (DE3) *Escherichia coli* cells, and the protein expression was induced with 0.2 mM isopropyl-β-D-thiogalactopyranoside (IPTG) at 16 °C for 16 h. The His-tagged protein was purified by affinity beads Ni-NTA, and then, the elution from Ni-NTA was purified by Q ion-exchange chromatography. The protein was further purified with gel filtration (Superdex 200 Increase, GE Healthcare) balanced with 20 mM Tris−HCl, pH 8.5, 300 mM NaCl, and 5% (w/w) glycerol. Finally, the purified protein was concentrated and stored at −80 °C. The expression and purification procedures of SARS-CoV-2 PLpro mutant C111S and human ISG15 are the same as PLpro.

Derivative Preparation. The derivatives of TSS and chloroxine were derived from similar structures in the PubChem database. The CAS numbers of compounds **1–12** are 115841-09-3, 7682221-4, 568-73-0, 568-72-9, 35825-57-1, 87205-99-0, 521-74-4, 54-05-8, 130-26-7, 130-16-5, 747408-78-2, and 57334-36-8, respectively. These compounds were purchased from Shanghai Target MoI, China (purity of 99.8% by HPLC and ^{1}H NMR spectrum).

Protease Activity Assay Based on the AMC Probe. The protease-activity assay by the AMC probe was developed previously.[28] Briefly, the protease-activity assay employed a fluorescent probe, ALKGG-AMC, based on the conserved amino acid sequence of the cleavage active site. The successful cleavage of the fluorescent probe by PLpro will lead to the release of the AMC fluorophore that can be detected by a specific 340 nm fluorescence signal. The AMC fluorescent peptide was prepared at a final concentration of 20 μM in the buffer of 50 mM HEPES sodium, pH 7.5, 5 mM DTT, and 0.1 mg/mL BSA. The PLpro protein was prepared at 1:2 dilutions in the buffer. Then, 50 μL of AMC fluorescent peptide and 50 μL of PLpro were reacted in a black 96-well plate (Greiner). After 10 min of incubation at room temperature, the fluorescence intensity was measured for 30 min on a BioTex Synergy HTX (Ex: 340 nm, Em: 460 nm). Two controls (without AMC fluorescent peptide or without PLpro) were performed along with other samples. Each compound (1 μL) was added into the reaction for testing its inhibition. Data was processed using GraphPad Prism 8.3.0.

PLpro-ISG15 Binding Analysis Based on Fluorescence Polarization. The binding assay by fluorescence polarization was developed previously.[28] Briefly, ISG15 was labeled with FITC according to the manual (Sigma, FITC CAS: 3326-32-7). Specifically, ISG15 and FITC were reacted in a molar ratio of 1:5. The FITC labeling efficiency was evaluated by the A495/A280 absorption (an acceptable A495/A280 ratio between 0.6 and 1.0). Afterward, 50 μL of ISG15-FITC and 50 μL of PLpro were reacted in a black 96-well plate (Greiner) with the buffer of 25 mM NaH$_2$PO$_4$, pH 7.5, 150 mM NaCl, 0.01% BSA, and 7.5 μM ZnCl$_2$. After 1 h of incubation at room temperature, the fluorescence signals were detected by a Tecan Spark (Ex: 485 nm, Em: 535 nm, G factor: 1). Two controls (without ISG15-FITC or without PLpro) were performed along with other samples. Data was processed using GraphPad Prism 8.3.0.

Docking Structure Preparation. The 3D structures of compounds **1–12** were downloaded from PubChem. The CIDs of compounds **1–12** are 1399150, 11600642, 114917, 164676, 160254, 11425923, 2453, 2719, 2788, 2817, 10016012, and 384164, respectively. PLpro structures were obtained from PDB: 6XAA (SARS-CoV-2 PLpro in complex with ubiquitin propargylamide) and PDB: 6XA9 (in complex with ISG15 C-terminal domain propargylamide).[25]

Docking. MGLTools v1.5.6 was employed for adding polar hydrogen atoms to PLpro and compounds and setting the rotatable bonds of each docking compound. The solvent and ligand moieties contained in the original protein crystal structure were removed to determine the available docking space. A docking grid space was built to cover all potential binding sites on the PLpro surface, and the grid point spacing was set to 1 Å with boxes of 52 Å × 82 Å × 66 Å for 6XA9_A and 60 Å × 82 Å × 70 Å for 6XAA_A. Docking was performed with AutoDock Vina v1.1.2. The number of runs for each

docking setup was 200, and binding affinity was determined and reported in kcal/mol.

MD Simulation. A representative conformation was selected from the above docking results for 200 ns molecular dynamics simulations. All ligand topologies were prepared under the ACPYPE force field. Proteins were converted to the GROMACS format with ParmED, and topologies were prepared with Ambertools20. Solvation and ionization brought the salt concentration to 150 mM. Energy minimization was performed to ensure that the water molecules were optimally arranged around PLpro. All computations were run on a high-performance cluster in the Shenzhen Bay Laboratory.

Thermal Shift Assay (TSA). Thermal stabilities of PLpro in the presence of compounds **1–12** at various pH buffers were analyzed in a 20 μL system in an optical 8-cap strip (MicroAmp). The final protein concentration was 0.2 mg/mL, and the molar ratio of protein to compound was 1:1.2. After addition of the protein-compound mixture, the fluorescent dye SYPRO Orange (Sigma) was added to each sample well. Real-time fluorescence data were collected on StepOnePlus with StepOne v2.3 (Thermo Fisher Scientific). The experiment type was melt curve, Rox was selected as the fluorescence channel, the temperature was set from 25 to 90 °C, and the data collection was at a 1 °C interval. An equal volume of DMSO to the compound was used as a control group, and all samples were set up in triplicate. Data was processed by GraphPad Prism 8.3.0.

Surface Plasmon Resonance (SPR). The binding kinetics of compound **7** to PLpro was measured by surface plasmon resonance on a Plex Array high-throughput molecular interaction instrument (PLEXERA, America) and a 3D photocross-linking chip. The compound was immobilized on the chip and then photocross-linked at a wavelength of 365 nm for 15 min followed by washing with *N,N*-dimethylformamide, ethanol, and pure water for 15 min sequentially. All injections were done at a flow rate of 2 μL/s and 20 °C. Both the association and dissociation phases were run for 300 s. The instrument was equilibrated with 600 μL of 10 mM glycine (pH 2.0) prior to injection of each compound. Data were fitted by BIAevaluation software using a 1:1 binding model.

Antiviral Assays. WT, delta, and omicron of SARS-CoV-2 were propagated in Vero E6 cells. For the IFA, the virus (MOI of 0.05) was first co-incubated with a serially diluted compound for 1 h at 37 °C. Fifty microliters of mixtures was then transferred to pre-seeded Vero E6 cells (ATCC, 1.5×10^4 cells per well) in a 96-well plate for 1 h at 37 °C to allow infection. The mixtures were removed and covered with the maintenance medium (DMEM containing 2% FBS) containing serially diluted compounds for 24 h at 37 °C. Cells were fixed with 4% paraformaldehyde solution for 1 h at room temperature before further IFA detection. After being permeabilized with 0.2% Triton X-100 for 30 min, cells were co-incubated with SARS-CoV/SARS-CoV-2 Nucleocapsid Rabbit PAb (Sino Biological, 40143-T62) as the primary antibody and Alexa Fluor 488 AffiniPure Donkey Anti-Rabbit IgG (H + L) (Jackson, 711-545-152) as the secondary antibody. Nuclei were stained with DAPI. The SARS-CoV-2 specific fluorescence intensity signal was collected and read by a Nexcelom Celigo imaging cytometer for virus inhibition analysis.

For the cytotoxicity assay, Vero E6 (1.5×10^4 per well) was pre-incubated in 96-well plates for 24 h at 37 °C, 5% CO$_2$. The compounds were then introduced in various concentrations.

The relative number of viable cells was assessed after 24 h according to the CCK-8 kit's instructions (Yeasen, China).

ASSOCIATED CONTENT

Supporting Information

The Supporting Information is available free of charge at https://pubs.acs.org/doi/10.1021/acsomega.2c06675.

^{1}H NMR and HPLC reports of compounds (PDF)

Further details of molecular docking (Figures S1 and S2 and Table S1) and MD simulation (Figures S3, S4, and S7); thermal melt curves of compounds **1−12** with PLpro (Figure S5); positive control group for the IFA-based antiviral assay (Figure S6); compound information (Table S2) (PDF)

AUTHOR INFORMATION

Corresponding Authors

Jincun Zhao − *Guangzhou Eighth People's Hospital, Guangzhou Medical University, Guangzhou, Guangdong 510060, China; State Key Laboratory of Respiratory Disease, National Clinical Research Centre for Respiratory Disease, Guangzhou Institute of Respiratory Health, the First Affiliated Hospital of Guangzhou Medical University, Guangzhou, Guangdong 511436, China; Guangzhou Laboratory, Bio-island, Guangzhou, Guangdong 510320, China; Shanghai Institute for Advanced Immunochemical Studies, School of Life Science and Technology, ShanghaiTech University, Shanghai 201210, China;* Email: zhaojincun@gird.cn

Yaoqi Zhou − *Institute for Systems and Physical Biology, Shenzhen Bay Laboratory, Shenzhen, Guangdong 518038, China; Shenzhen Graduate School, Peking University, Shenzhen, Guangdong 518055, China;* orcid.org/0000-0002-9958-5699; Email: zhouyq@szbl.ac.cn

Jian Zhan − *Institute for Systems and Physical Biology, Shenzhen Bay Laboratory, Shenzhen, Guangdong 518038, China;* Email: zhanjian@szbl.ac.cn

Wei Xu − *Guangdong Provincial Key Laboratory of New Drug Screening, School of Pharmaceutical Sciences, Southern Medical University, Guangzhou 510515, China; Guangzhou Eighth People's Hospital, Guangzhou Medical University, Guangzhou, Guangdong 510060, China;* orcid.org/0000-0002-3135-5010; Email: xuwei3322@smu.edu.cn

Authors

Xin Chen − *Guangdong Provincial Key Laboratory of New Drug Screening, School of Pharmaceutical Sciences, Southern Medical University, Guangzhou 510515, China; Guangzhou Eighth People's Hospital, Guangzhou Medical University, Guangzhou, Guangdong 510060, China*

Ke Chen − *Institute for Systems and Physical Biology, Shenzhen Bay Laboratory, Shenzhen, Guangdong 518038, China; Shenzhen Graduate School, Peking University, Shenzhen, Guangdong 518055, China*

Zhaoyong Zhang − *State Key Laboratory of Respiratory Disease, National Clinical Research Centre for Respiratory Disease, Guangzhou Institute of Respiratory Health, the First Affiliated Hospital of Guangzhou Medical University, Guangzhou, Guangdong 511436, China*

Peilan Wei − *State Key Laboratory of Respiratory Disease, National Clinical Research Centre for Respiratory Disease, Guangzhou Institute of Respiratory Health, the First Affiliated Hospital of Guangzhou Medical University, Guangzhou, Guangdong 511436, China*

Lu Zhang − *Guangzhou Customs District Technology Centre, Guangzhou, Guangdong 510623, China*

Yunxia Xu − *Guangdong Provincial Key Laboratory of New Drug Screening, School of Pharmaceutical Sciences, Southern Medical University, Guangzhou, Guangdong 510515, China*

Qili Lun − *Guangdong Provincial Key Laboratory of New Drug Screening, School of Pharmaceutical Sciences, Southern Medical University, Guangzhou, Guangdong 510515, China*

Yanhong Ma − *Guangdong Provincial Key Laboratory of New Drug Screening, School of Pharmaceutical Sciences, Southern Medical University, Guangzhou, Guangdong 510515, China*

Fang Wu − *Guangdong Provincial Key Laboratory of New Drug Screening, School of Pharmaceutical Sciences, Southern Medical University, Guangzhou, Guangdong 510515, China*

Ying Zhang − *Guangdong Provincial Key Laboratory of New Drug Screening, School of Pharmaceutical Sciences, Southern Medical University, Guangzhou, Guangdong 510515, China*

Yanqun Wang − *State Key Laboratory of Respiratory Disease, National Clinical Research Centre for Respiratory Disease, Guangzhou Institute of Respiratory Health, the First Affiliated Hospital of Guangzhou Medical University, Guangzhou, Guangdong 511436, China*

Complete contact information is available at: https://pubs.acs.org/10.1021/acsomega.2c06675

Author Contributions

◆X.C., K.C., Z.W., and P.W. contributed equally.

Notes

The authors declare no competing financial interest.

ACKNOWLEDGMENTS

ABBREVIATIONS

SARs	structure−activity relationships
FPA	fluorescence polarization assay
MDs	molecular dynamics simulations
RdRP	RNA-dependent RNA polymerase
TSS	tanshinone IIA sulfonate sodium
AMC	aminomethyl-coumarin
SARS-CoV-2	severe acute respiratory syndrome coronavirus 2
IC$_{50}$	concentration of 50% inhibition
EC$_{50}$	concentration for 50% of the maximal effect
TSA	thermal shift assay
IFA	immunofluorescence assay
BSL-3	biological safety level-3
SPR	surface plasmon resonance
PDB	protein data bank

■ REFERENCES

(1) V'kovski, P.; Kratzel, A.; Steiner, S.; Stalder, H.; Thiel, V. Coronavirus biology and replication: implications for SARS-CoV-2. *Nat. Rev. Microbiol.* **2021**, *19*, 155−170.

(2) Wölfel, R.; Corman, V. M.; Guggemos, W.; Seilmaier, M.; Zange, S.; Müller, M. A.; Niemeyer, D.; Jones, T. C.; Vollmar, P.; Rothe, C.; Hoelscher, M.; Bleicker, T.; Brünink, S.; Schneider, J.; Ehmann, R.; Zwirglmaier, K.; Drosten, C.; Wendtner, C. Virological assessment of hospitalized patients with COVID-2019. *Nature* **2020**, *581*, 465−469.

(3) Xu, Z.; Shi, L.; Wang, Y.; Zhang, J.; Huang, L.; Zhang, C.; Liu, S.; Zhao, P.; Liu, H.; Zhu, L.; Tai, Y.; Bai, C.; Gao, T.; Song, J.; Xia, P.; Dong, J.; Zhao, J.; Wang, F.-S. Pathological findings of COVID-19 associated with acute respiratory distress syndrome. *Lancet Respir. Med.* **2020**, *8*, 420−422.

(4) Guan, W.-J.; Ni, Z.-Y.; Hu, Y.; Liang, W.-H.; Ou, C.-Q.; He, J.-X.; Liu, L.; Shan, H.; Lei, C.-L.; Hui, D. S. C.; Du, B.; Li, L.-J.; Zeng, G.; Yuen, K.-Y.; Chen, R.-C.; Tang, C.-L.; Wang, T.; Chen, P.-Y.; Xiang, J.; Li, S.-Y.; Wang, J.-L.; Liang, Z.-J.; Peng, Y.-X.; Wei, L.; Liu, Y.; Hu, Y.-H.; Peng, P.; Wang, J.-M.; Liu, J.-Y.; Chen, Z.; Li, G.; Zheng, Z.-J.; Qiu, S.-Q.; Luo, J.; Ye, C.-J.; Zhu, S.-Y.; Zhong, N.-S. Clinical Characteristics of Coronavirus Disease 2019 in China. *N. Engl. J. Med.* **2020**, *382*, 1708−1720.

(5) Yuen, K.-S.; Ye, Z.-W.; Fung, S.-Y.; Chan, C.-P.; Jin, D.-Y. SARS-CoV-2 and COVID-19: The most important research questions. *Cell Biosci.* **2020**, *10*, 40.

(6) Hall, D. C., Jr.; Ji, H.-F. A search for medications to treat COVID-19 via in silico molecular docking models of the SARS-CoV-2 spike glycoprotein and 3CL protease. *Travel Med. Infect. Dis.* **2020**, *35*, No. 101646.

(7) Wang, M.; Cao, R.; Zhang, L.; Yang, X.; Liu, J.; Xu, M.; Shi, Z.; Hu, Z.; Zhong, W.; Xiao, G. Remdesivir and chloroquine effectively inhibit the recently emerged novel coronavirus (2019-nCoV) in vitro. *Cell Res.* **2020**, *30*, 269−271.

(8) Xu, X.; Han, M.; Li, T.; Sun, W.; Wang, D.; Fu, B.; Zhou, Y.; Zheng, X.; Yang, Y.; Li, X.; Zhang, X.; Pan, A.; Wei, H. Effective treatment of severe COVID-19 patients with tocilizumab. *Proc. Natl. Acad. Sci. U. S. A.* **2020**, *117*, 10970−10975.

(9) Drożdżal, S.; Rosik, J.; Lechowicz, K.; Machaj, F.; Kotfis, K.; Ghavami, S.; Łos, M. J. FDA approved drugs with pharmacotherapeutic potential for SARS-CoV-2 (COVID-19) therapy. *Drug Resistance Updates* **2020**, *53*, No. 100719.

(10) Kamat, S.; Kumari, M. Repurposing Chloroquine Against Multiple Diseases With Special Attention to SARS-CoV-2 and Associated Toxicity. *Front. Pharmacol.* **2021**, *12*, No. 576093.

(11) Ma, C.; Sacco, M. D.; Hurst, B.; Townsend, J. A.; Hu, Y.; Szeto, T.; Zhang, X.; Tarbet, B.; Marty, M. T.; Chen, Y.; Wang, J. Boceprevir, GC-376, and calpain inhibitors II, XII inhibit SARS-CoV-2 viral replication by targeting the viral main protease. *Cell Res.* **2020**, *30*, 678−692.

(12) Li, G.; De Clercq, E. Therapeutic options for the 2019 novel coronavirus (2019-nCoV). *Nat. Rev. Drug Discovery* **2020**, *19*, 149−150.

(13) Yu, R.; Chen, L.; Lan, R.; Shen, R.; Li, P. Computational screening of antagonists against the SARS-CoV-2 (COVID-19) coronavirus by molecular docking. *Int. J. Antimicrob. Agents* **2020**, *56*, No. 106012.

(14) Russo, M.; Moccia, S.; Spagnuolo, C.; Tedesco, I.; Russo, G. L. Roles of flavonoids against coronavirus infection. *Chem.-Biol. Interact.* **2020**, *328*, No. 109211.

(15) Huang, F.; Li, Y.; Leung, E. L.-H.; Liu, X.; Liu, K.; Wang, Q.; Lan, Y.; Li, X.; Yu, H.; Cui, L.; Luo, H.; Luo, L. A review of therapeutic agents and Chinese herbal medicines against SARS-COV-2 (COVID-19). *Pharmacol. Res.* **2020**, *158*, No. 104929.

(16) Huang, Y.-F.; Bai, C.; He, F.; Xie, Y.; Zhou, H. Review on the potential action mechanisms of Chinese medicines in treating Coronavirus Disease 2019 (COVID-19). *Pharmacol. Res.* **2020**, *158*, No. 104939.

(17) Syed, Y. Y. Molnupiravir: First Approval. *Drugs* **2022**, *82*, 455−460.

(18) Painter, G. R.; Natchus, M. G.; Cohen, O.; Holman, W.; Painter, W. P. Developing a direct acting, orally available antiviral agent in a pandemic: the evolution of molnupiravir as a potential treatment for COVID-19. *Curr. Opin. Virol.* **2021**, *50*, 17−22.

(19) Hashemian, S. M. R.; Pourhanifeh, M. H.; Hamblin, M. R.; Shahrzad, M. K.; Mirzaei, H. RdRp inhibitors and COVID-19: Is molnupiravir a good option? *Biomed. Pharmacother.* **2022**, *146*, No. 112517.

(20) Liu, C.; Zhou, Q.; Li, Y.; Garner, L. V.; Watkins, S. P.; Carter, L. J.; Smoot, J.; Gregg, A. C.; Daniels, A. D.; Jervey, S.; Albaiu, D. Research and Development on Therapeutic Agents and Vaccines for COVID-19 and Related Human Coronavirus Diseases. *ACS Cent. Sci.* **2020**, *6*, 315−331.

(21) Isaacson, M. K.; Ploegh, H. L. Ubiquitination, ubiquitin-like modifiers, and deubiquitination in viral infection. *Cell Host Microbe* **2009**, *5*, 559−570.

(22) Yuen, C.-K.; Lam, J.-Y.; Wong, W.-M.; Mak, L.-F.; Wang, X.; Chu, H.; Cai, J.-P.; Jin, D.-Y.; To, K. K.-W.; Chan, J. F.-W.; Yuen, K.-Y.; Kok, K.-H. SARS-CoV-2 nsp13, nsp14, nsp15 and orf6 function as potent interferon antagonists. *Emerging Microbes Infect.* **2020**, *9*, 1418−1428.

(23) Freitas, B. T.; Durie, I. A.; Murray, J.; Longo, J. E.; Miller, H. C.; Crich, D.; Hogan, R. J.; Tripp, R. A.; Pegan, S. D. Characterization and Noncovalent Inhibition of the Deubiquitinase and deISGylase Activity of SARS-CoV-2 Papain-Like Protease. *ACS Infect. Dis.* **2020**, *6*, 2099−2109.

(24) Rao, P.; Patel, R.; Shukla, A.; Parmar, P.; Rawal, R. M.; Saraf, M.; Goswami, D. Identifying structural-functional analogue of GRL0617, the only well-established inhibitor for papain-like protease (PLpro) of SARS-CoV2 from the pool of fungal metabolites using docking and molecular dynamics simulation. *Mol. Diversity* **2022**, 309.

(25) Klemm, T.; Ebert, G.; Calleja, D. J.; Allison, C. C.; Richardson, L. W.; Bernardini, J. P.; Lu, B. G. C.; Kuchel, N. W.; Grohmann, C.; Shibata, Y.; Gan, Z. Y.; Cooney, J. P.; Doerflinger, M.; Au, A. E.; Blackmore, T. R.; van der Heden van Noort, G. J.; Geurink, P. P.; Ovaa, H.; Newman, J.; Riboldi-Tunnicliffe, A.; Czabotar, P. E.; Mitchell, J. P.; Feltham, R.; Lechtenberg, B. C.; Lowes, K. N.; Dewson, G.; Pellegrini, M.; Lessene, G.; Komander, D. Mechanism and inhibition of the papain-like protease, PLpro, of SARS-CoV-2. *EMBO J.* **2020**, *39*, No. e106275.

(26) Fu, Z.; Huang, B.; Tang, J.; Liu, S.; Liu, M.; Ye, Y.; Liu, Z.; Xiong, Y.; Zhu, W.; Cao, D.; Li, J.; Niu, X.; Zhou, H.; Zhao, Y. J.; Zhang, G.; Huang, H. The complex structure of GRL0617 and SARS-CoV-2 PLpro reveals a hot spot for antiviral drug discovery. *Nat. Commun.* **2021**, *12*, 488.

(27) Ma, C.; Sacco, M. D.; Xia, Z.; Lambrinidis, G.; Townsend, J. A.; Hu, Y.; Meng, X.; Szeto, T.; Ba, M.; Zhang, X.; Gongora, M.; Zhang, F.; Marty, M. T.; Xiang, Y.; Kolocouris, A.; Chen, Y.; Wang, J. Discovery of SARS-CoV-2 Papain-like Protease Inhibitors through a Combination of High-Throughput Screening and a FlipGFP-Based Reporter Assay. *ACS Cent. Sci.* **2021**, *7*, 1245−1260.

(28) Xu, Y.; Chen, K.; Pan, J.; Lei, Y.; Zhang, D.; Fang, L.; Tang, J.; Chen, X.; Ma, Y.; Zheng, Y.; Zhang, B.; Zhou, Y.; Zhan, J.; Xu, W. Repurposing clinically approved drugs for COVID-19 treatment targeting SARS-CoV-2 papain-like protease. *Int. J. Biol. Macromol.* **2021**, *188*, 137−146.

(29) Xu, M.-J.; Jiang, L.-F.; Wu, T.; Chu, J.-H.; Wei, Y.-D.; Aa, J.-Y.; Wang, G.-J.; Hao, H.-P.; Ju, W.-Z.; Li, P. Inhibitory Effects of Danshen components on CYP2C8 and CYP2J2. *Chem.-Biol. Interact.* **2018**, *289*, 15−22.

(30) Biesiada, J.; Porollo, A.; Velayutham, P.; Kouril, M.; Meller, J. Survey of public domain software for docking simulations and virtual screening. *Hum. Genomics* **2011**, *5*, 497−505.

(31) Han, Y.; Duan, X.; Yang, L.; Nilsson-Payant, B. E.; Wang, P.; Duan, F.; Tang, X.; Yaron, T. M.; Zhang, T.; Uhl, S.; Bram, Y.; Richardson, C.; Zhu, J.; Zhao, Z.; Redmond, D.; Houghton, S.; Nguyen, D.-H. T.; Xu, D.; Wang, X.; Jessurun, J.; Borczuk, A.; Huang, Y.; Johnson, J. L.; Liu, Y.; Xiang, J.; Wang, H.; Cantley, L. C.; tenOever, B. R.; Ho, D. D.; Pan, F. C.; Evans, T.; Chen, H. J.;

Schwartz, R. E.; Chen, S. Identification of SARS-CoV-2 inhibitors using lung and colonic organoids. *Nature* **2021**, *589*, 270−275.

(32) Shan, H.; Liu, J.; Shen, J.; Dai, J.; Xu, G.; Lu, K.; Han, C.; Wang, Y.; Xu, X.; Tong, Y.; Xiang, H.; Ai, Z.; Zhuang, G.; Hu, J.; Zhang, Z.; Li, Y.; Pan, L.; Tan, L. Development of potent and selective inhibitors targeting the papain-like protease of SARS-CoV-2. *Cell Chem. Biol.* **2021**, *28*, 855.

(33) Shin, D.; Mukherjee, R.; Grewe, D.; Bojkova, D.; Baek, K.; Bhattacharya, A.; Schulz, L.; Widera, M.; Mehdipour, A. R.; Tascher, G.; Geurink, P. P.; Wilhelm, A.; van der Heden van Noort, G. J.; Ovaa, H.; Müller, S.; Knobeloch, K.-P.; Rajalingam, K.; Schulman, B. A.; Cinatl, J.; Hummer, G.; Ciesek, S.; Dikic, I. Papain-like protease regulates SARS-CoV-2 viral spread and innate immunity. *Nature* **2020**, *587*, 657−662.